An LSTM-GNN-Based Early Warning System for Laboratory Biosafety Using BIM and IoT-Driven Multi-Source Data Fusion

Jun Cao
General Support Department, Shanghai Center for Disease Control and Prevention, Shanghai, 201107, China.
Corresponding Email: caojun2@scdc.sh.cn

Keywords: Laboratory biosafety; BIM technology; IoT monitoring; multi-source heterogeneous data fusion; LSTM-GNN algorithm; dynamic early warning

Received: September 4, 2025

To address the challenges of traditional laboratory biosafety monitoring (e.g., data lag, single-dimensionality, rigid early warning), this paper designs an integrated system combining "BIM + IoT + LSTM-GNN Intelligent Algorithm" with a four-layer "Perception-Transmission-Platform-Application" architecture. Hardware includes the SHT35 temperature and humidity sensor (±0.1°C/±2% RH), BV6000 pathogen sensor (0.01 CFU/mL lower limit), and UWB positioning tags (0.3–1m accuracy). Software adopts a MySQL+Redis database, and a dynamic early warning algorithm integrating an improved attention mechanism, LSTM (for temporal feature extraction), and GNN (for spatial correlation mining) is proposed. Experiments were conducted on 15,000 datasets (covering 10 scenarios) with three control systems: traditional threshold system, single LSTM system, and IoT static monitoring system. Key results include: (1) Temperature-humidity error rates: 0.5% (normal scenarios), 0.7% (mild abnormal), 0.8% (severe abnormal); (2) Response time: 0.3s for 10,000 datasets; (3) Early warning accuracy: 98.5% (false positive rate 1.2%, false negative rate 0.3%); (4) 72-hour data transmission success rate: 99.9%. SPSS significance analysis ($p<0.01$) confirms the system outperforms control solutions, fully meeting laboratories' dynamic safety management needs.

Povzetek: Predstavljen je inteligentni sistem za laboratorijsko biosigurnost (BIM + IoT + LSTM-GNN), ki z dinamičnim zgodnjim opozarjanjem doseže 98,5 % natančnost in zelo hiter odziv (0,3 s).

1 Introduction

With the rapid development of biomedicine and microbiology, laboratories face increasingly urgent biosafety risk prevention needs. According to the "Global Laboratory Biosafety Incident Statistics Report (2020-2024)", 327 incidents occurred worldwide in five years—42% from pathogenic microorganism leaks and 28% from sample contamination due to abnormal temperature and humidity. These incidents invalidate research data and threaten operator health and the surrounding environment. However, traditional monitoring relies on manual inspections and single-sensor tracking, leading to three critical issues: data collection lag (1.5–3 hours on average), limited monitoring dimensions (only basic parameters like temperature/humidity), and rigid early warning mechanisms (fixed threshold triggers). This makes it difficult to meet the dynamic safety management requirements of complex scenarios.

Building Information Modeling (BIM) excels in 3D visualization and data integration, while the Internet of Things (IoT) establishes real-time "perception-transmission-analysis" data chains via multi-type sensors and high-speed networks. Their integration provides a new technical path for biosafety monitoring: BIM enables digital mapping of lab layouts and equipment, and IoT ensures real-time access to multi-source safety data, laying the foundation for dynamic early warning.

Looking at the current state of domestic and international research, foreign studies started earlier but have clear limitations. The LabSafe system (US CDC) monitors pathogen concentrations and personnel trajectories but lacks BIM technology and spatial data correlation analysis, failing to link risks to specific lab locations [2]. Merck KGaA's (Germany) BioMonitor system offers basic early warning but uses a single LSTM model, which cannot integrate multi-source heterogeneous data (e.g., discrete personnel location data and continuous temperature data) or capture spatial dependencies between parameters [3]. Domestic research also has gaps: Tsinghua University's "IoT + Laboratory Safety Monitoring Solution" realizes real-time collection of temperature, humidity, and access control data but omits core biological parameters like pathogen concentration, limiting its ability to detect biological risks

[4]. Shanghai Jiao Tong University's BIM-based lab management system focuses on spatial resource scheduling (e.g., equipment allocation) and lacks a dynamic safety early warning module, unable to respond to real-time risk changes [5].

In general, existing research has not formed an integrated "BIM + IoT + Intelligent Algorithm" monitoring system. Key technical gaps include: (1) Insufficient deep fusion of multi-source heterogeneous data—most systems process single-type data independently, ignoring the coupling between temporal (e.g., temperature trends) and spatial (e.g., pathogen diffusion with personnel movement) features; (2) Low dynamic warning accuracy—fixed thresholds or single time-series models cannot adapt to complex scenarios (e.g., distinguishing temporary equipment fluctuations from true risks); (3) Lack of scalability evaluation—most experiments are conducted in small single-lab settings, ignoring performance in large-scale institutional environments with hundreds of labs [6]. Table 1 below compares core features and limitations of existing systems to further clarify gaps addressed by this study:

Table 1: Comparison of existing laboratory biosafety monitoring systems

System Name	Developer/Institution	Parameter Coverage	Dynamic Capability	Spatial Integration	Data Fusion Strategy	Limitations	Reference
LabSafe	US CDC	Pathogen concentration, personnel trajectory	Basic (fixed threshold)	No (no spatial mapping)	Single-type data processing	Lacks BIM; no spatial correlation analysis	[2]
BioMonitor	Merck KGaA (Germany)	Temperature, humidity, pathogen concentration	Dynamic (single LSTM)	No	Time-series data only	Cannot integrate heterogeneous data; no spatial features	[3]
IoT + Safety Solution	Tsinghua University	Temperature, humidity, access control	Static monitoring	No	Independent data collection	Omits pathogen monitoring; no early warning	[4]
BIM-based Lab Management	Shanghai Jiao Tong University	Spatial layout, equipment status	No dynamic warning	Yes (BIM mapping)	No data fusion	Focuses on resource management; no safety alerts	[5]
Proposed System	This study	Temperature, humidity, pathogen, personnel location	Dynamic (attention-LSTM-GNN)	Yes (BIM + spatial correlation)	Multi-source fusion (temporal + spatial)	Needs optimization for extreme low temperatures	This study

The main contents of this study include: (1) Designing a four-layer "Perception-Transmission-Platform-Application" architecture, clarifying hardware selection and software module functions; (2) Proposing a multi-source heterogeneous data dynamic warning algorithm integrating an improved attention mechanism, LSTM, and GNN to enhance accuracy and adaptability; (3) Building an experimental platform to verify performance via comparative tests with mainstream systems. To address existing gaps, this study explicitly answers three research questions:

1. How to design a four-layer architecture to overcome traditional hardware limitations in data collection accuracy and transmission stability?
2. How to integrate an attention-LSTM-GNN model to realize deep fusion of multi-source heterogeneous data and improve dynamic early warning accuracy?
3. How to verify the system's scalability in large-scale lab settings and generalizability across diverse environmental conditions?

The research follows the logical process: "demand analysis → system design (hardware + software) → algorithm development → simulation experiment (with 5-fold cross-validation) → result verification → conclusion

and prospect" to ensure scientific rigor.

2 Overall system design

Laboratory biosafety monitoring must balance real-time data, accurate warnings, and operational stability. Therefore, the overall system design must be demand-driven, forming a complete technical solution through architecture planning, hardware matching, and software development [5]. This chapter begins with a requirements analysis and gradually develops the architecture, hardware, and software design to ensure that each component synergizes to meet laboratory safety management requirements.

2.1 System requirements analysis

System requirements are defined from three core dimensions: functionality, performance, and security, providing a clear basis for subsequent design [6]. Functional requirements require real-time monitoring of multiple parameters, covering three key indicators: temperature and humidity, pathogen concentration, and personnel location. Furthermore, dynamic warnings (triggering low, medium, or high alerts based on risk level), data visualization (linked display with BIM models), and historical traceability (supporting data query within one year) are required to meet the needs of daily laboratory management and emergency response. In terms of performance requirements, combined with the laboratory's safety and control accuracy requirements, the temperature and humidity monitoring accuracy must reach ±0.1°C/±2% RH, the pathogen concentration detection limit must be no higher than 0.01 CFU/mL, and personnel positioning accuracy must be controlled within 0.3m to 1m. Regarding response efficiency, the average response time from data collection to alert triggering must be ≤0.3s to ensure timely handling of risk events [7]. During continuous system operation, the data transmission success rate must be ≥99.9% to avoid monitoring failures due to data interruptions. Security requirements focus on the data and the system itself. Data transmission must utilize the AES-256 encryption algorithm to prevent leakage, and user permissions must be managed hierarchically based on "administrator - operator - guest." Furthermore, the system must resist electromagnetic interference to accommodate the complex electromagnetic environment of the laboratory.

2.2 System architecture design

Based on these requirements, a four-layer architecture consisting of "perception - transmission - platform - application" was constructed, with each layer having clear responsibilities and coordinated linkage. The perception layer serves as the data collection portal, deploying sensors such as temperature and humidity, pathogen concentration, and personnel location, responsible for converting physical safety parameters into processable digital signals [8]. The transmission layer is responsible for data transfer, utilizing a 5G + edge computing convergence solution to achieve high-speed data transmission via a 5G private network. Edge computing nodes process some data locally to reduce latency and ensure real-time data availability. The platform layer is the core hub of the system. It uses BIM technology to construct a three-dimensional digital model of the laboratory, visually linking monitoring points to spatial locations [9]. Furthermore, a data fusion module cleans and integrates multi-source heterogeneous data, providing high-quality data for subsequent warnings. The application layer provides interactive functions for users, including dynamic monitoring, warning management, data statistics, and emergency decision-making modules, meeting the operational needs of different roles. This four-layer architecture forms a closed loop of "acquisition - transmission - processing - application," ensuring efficient operation of the entire system process, from data acquisition to decision output.

2.3 System hardware design

Hardware is the physical foundation of system operation. Design must focus on the goals of "stable data collection, efficient transmission, and reliable processing," encompassing three aspects: equipment selection, deployment planning, and communication design.

2.3.1 Hardware device selection

Hardware device selection must match monitoring parameter accuracy and scenario adaptability. Modules are categorized by function, clearly presenting each device model and core parameters. Environmental monitoring includes the SHT35 temperature and humidity sensor and the BioVigilant BV6000 pathogen concentration sensor [10]. The former has a measurement range of -40°C to 125°C and an accuracy of ±0.1°C/±2% RH, enabling detection of subtle changes in laboratory environments. The latter has a detection limit of 0.01 CFU/mL and supports real-time bacterial counts, meeting pathogen risk monitoring requirements. Personnel positioning uses UWB positioning tags, offering an accuracy of 0.3m to 1m and a battery life of ≥72 hours. These tags can track personnel locations in real time to identify violations. Data processing includes the NVIDIA Jetson AGX Xavier edge computing node and the Dell PowerEdge R750 server. The edge node has an 8-core ARM v8.2 CPU and a 512-core Volta architecture. GPUs can rapidly process real-time data from multiple sources. Servers equipped with dual Intel Xeon Gold 6348 CPUs and 128GB of DDR4 memory ensure data storage and stable system operation. Communications equipment utilizes a 5G industrial router and a 24-port Gigabit PoE switch. The router supports both SA and NSA modes, with downlink speeds ≥ 1Gbps and uplink speeds ≥

200Mbps. The switch supports PoE power, simplifying sensor wiring. Together, these two enable high-speed communication between hardware devices.

2.3.2 Hardware deployment planning

Hardware deployment should be integrated with laboratory space layout and monitoring priorities, adopting a strategy of "densifying core areas and fully covering public areas." In core laboratory areas (biosafety cabinet operating areas and sample refrigerated storage areas), one SHT35 temperature and humidity sensor and one BioVigilant BV6000 pathogen sensor are deployed every 5 square meters to ensure comprehensive monitoring of parameters in critical areas. At high-traffic areas such as laboratory entrances, exits, and corridor corners, one UWB positioning base station is deployed every 10 meters, requiring a total of 4 to 6 base stations to form a positioning network and capture personnel location information in real time. Edge computing nodes are deployed in the laboratory computer room and directly connected to each sensor via a PoE switch, shortening data transmission distance and reducing latency [11]. Servers are deployed in the laboratory management center computer room and establish dedicated communication links with the edge computing nodes via 5G routers to avoid transmission interference caused by sharing bandwidth with other networks. The management center computer room is also equipped with a UPS to ensure normal operation of the servers in the event of a power outage.

2.3.3 Hardware communication design

Hardware communication utilizes a three-tier architecture: "sensor - edge computing node - server." The communication method between sensors and edge computing nodes is scenario-specific: fixed sensors (e.g., temperature/humidity) use RS-485 bus communication (transmission distance ≤1200m, baud rate 9600–115200bps), while mobile devices (e.g., UWB positioning tags) use Wi-Fi 6 (transmission rate ≥9.6Gbps, latency ≤10ms), adapting to different installation needs [12].

Dual-link communication is adopted between edge computing nodes and servers: the primary link is a 5G private network (with QoS guarantee, latency ≤20ms), and the backup link is wired Ethernet (transmission rate up to 1Gbps, latency ≤5ms). This redundancy design ensures uninterrupted data transmission. All hardware devices support Modbus and MQTT protocols to standardize data formats and avoid parsing errors from protocol incompatibility. The lightweight nature of MQTT reduces device communication energy consumption and extends sensor battery life.

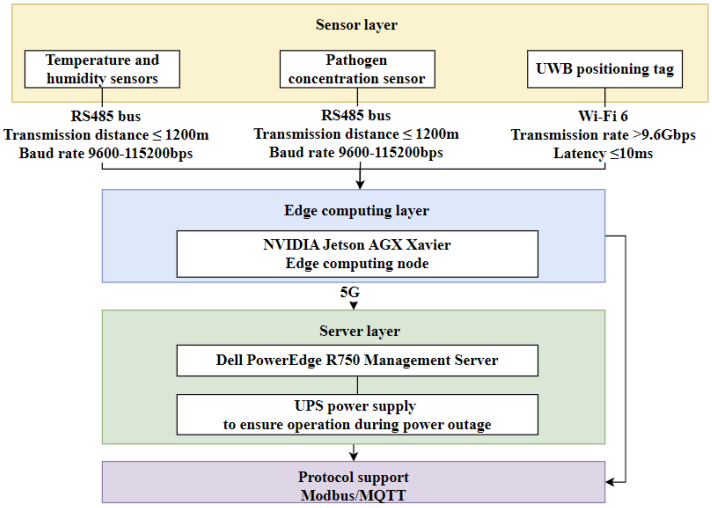

Figure 1: Hardware communication architecture module diagram.

2.4 System software design

2.4.1 Software module development

Software module development is organized using a four-layer architecture: "Perception - Transmission - Platform - Application." The module diagram (Figure 2) illustrates each layer's components and core functions: The perception layer software is developed in C language based on the FreeRTOS real-time operating system. Its core is the sensor data acquisition program, with a sampling frequency set to 1 per second [13]. It supports data caching and resumable transmission. When the network is interrupted, data can be temporarily stored and automatically retransmitted upon recovery, ensuring continuous data collection. The transport layer software is developed based on the Linux system. The communication management module integrates 5G and Ethernet communication drivers and embeds the AES-256 encryption algorithm to encrypt transmitted data. A flow control algorithm avoids data congestion and ensures secure and stable data transmission. The platform layer software is divided into two modules: BIM modelling and

data fusion. The BIM modelling module is developed based on the Revit API and supports constructing 3D laboratory models, spatial partition annotation, and visual binding of sensor locations. Real-time data from each monitoring point can be visually viewed in the model. The data fusion module is developed in Python and integrates Pandas. With the NumPy library, it realizes multi-source data format conversion, outlier elimination and feature extraction, providing standardized data for the early warning algorithm; the application layer software adopts the "Vue.js front-end + Spring Boot back-end" architecture, which includes four sub-modules: dynamic monitoring, early warning, data management, and emergency decision-making [14]. The dynamic monitoring module supports real-time data curve display and BIM model data linkage annotation. The early warning module integrates the multi-source heterogeneous data fusion early warning algorithm designed in this paper, and can push early warning information through pop-ups and SMS. The data management module supports historical data query, report generation and export. The emergency decision-making module has a built-in emergency plan library, which can automatically recommend disposal plans according to the warning level, fully meeting the laboratory management needs.

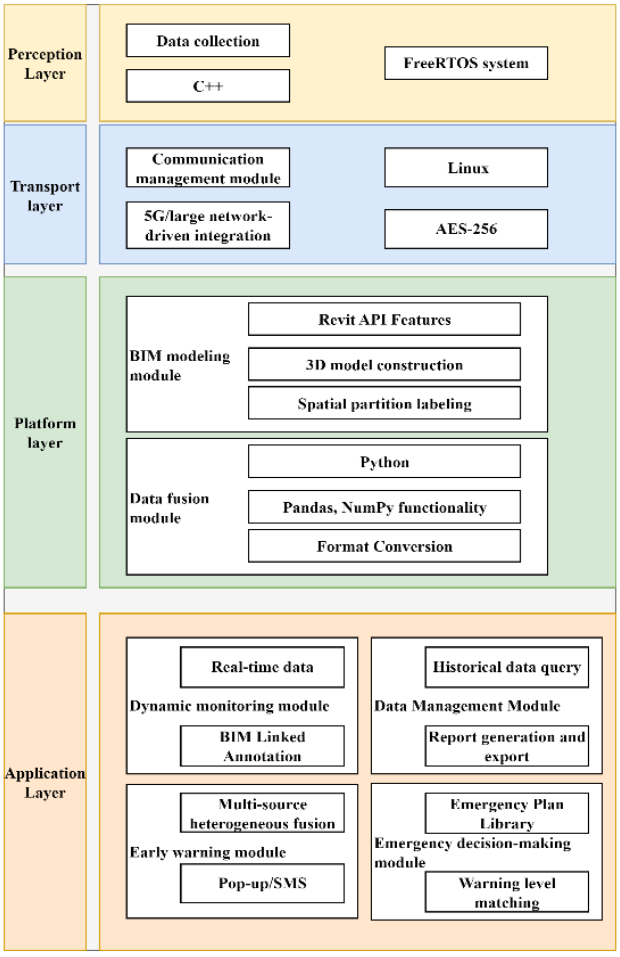

Figure 2: Software module development diagram.

2.4.2 Database design

The database uses a MySQL 8.0 relational database combined with a Redis cache architecture, balancing data storage stability and read/write efficiency. The basic information table stores static data such as laboratory space information (e.g., area number, area), sensor parameters (e.g., sensor ID, model, installation location), and user permissions (e.g., user ID, role, and operation permissions), serving as the foundation for system operation. The real-time monitoring data table stores real-time data such as temperature and humidity, pathogen concentration, and personnel location. It uses a time-based table partitioning strategy (generating one partition per hour), retaining only the most recent three months of data to reduce storage pressure [15]. The historical data table aggregates and archives real-time data daily, retaining one year of data and supporting compressed storage to facilitate long-term trend analysis. The warning information table stores information such as warning time, warning level, triggering cause (e.g., pathogen concentration exceeding the standard), and action results, providing a basis for subsequent safety reviews. Each data table is linked by primary key. For example, the real-time monitoring data table and the sensor table are linked by "sensor ID," the warning information table and the real-time monitoring data table are linked by "timestamp" to ensure data consistency. A data backup strategy is also designed: a full backup is automatically performed at 2:00 AM daily, and incremental backups are performed every 6 hours. Backup files are stored on an off-site server to prevent data loss due to hardware failure.

3 Dynamic warning algorithm for multi-source heterogeneous data fusion

3.1 Algorithm design background

Laboratory biosafety monitoring data exhibits significant multi-source heterogeneity: temperature and humidity data are continuous time series, pathogen concentration data exhibits pulsed fluctuations, and personnel location data are discrete spatial coordinates [16]. Furthermore, the sampling frequency (0.1-1 Hz) and accuracy of different sensor data vary significantly. Traditional early warning algorithms rely solely on fixed thresholds for a single parameter (e.g., a warning is issued when temperature or humidity exceeds 25°C), failing to capture the risks associated with multiple parameters. While single LSTM models can process time series data, they inadequately exploit spatial correlations (e.g., the coupling between pathogen concentration and personnel location), resulting in false alarm rates as high as 15%-20% and missed alarm rates exceeding 10%. Furthermore, dynamic changes in

laboratory scenarios (e.g., short-term increases in pathogen concentration during sample manipulation) can easily render fixed algorithms ineffective [17]. Therefore, designing a dynamic early warning algorithm that adapts to multi-source heterogeneous data and combines time series and spatial analysis capabilities is necessary.

3.2 Core concepts of the algorithm

Laboratory biosafety monitoring data exhibits significant multi-source heterogeneity: temperature/humidity are continuous time-series data, pathogen concentration shows pulsed fluctuations, and personnel location is discrete spatial coordinates [16]. Additionally, sensor sampling frequencies (0.1–1 Hz) and accuracy vary greatly. Traditional algorithms rely on single-parameter fixed thresholds (e.g., warning when temperature exceeds 25°C), failing to capture multi-factor risks. Single LSTM models process time-series data but ignore spatial correlations (e.g., coupling between pathogen concentration and personnel location), leading to false alarm rates of 15%–20% and missed alarm rates over 10%. Dynamic scenario changes (e.g., short-term pathogen concentration increases during sample handling) further reduce fixed-algorithm effectiveness [17]. Thus, an algorithm integrating temporal and spatial analysis capabilities is critical.

$$w_{i,t} = \frac{\exp\left(\alpha \cdot \frac{\left|x_{i,t} - \bar{x}_i\right|}{\sigma_i} + \beta \cdot r_{i,s}\right)}{\sum_{k=1}^{n} \exp\left(\alpha \cdot \frac{\left|x_{k,t} - \bar{x}_k\right|}{\sigma_k} + \beta \cdot r_{k,s}\right)} \tag{1}$$

In the formula, $w_{i,t}$ is the weight of the i category data at time t, $x_{i,t}$ is the real-time data, $\bar{x}_i, \sigma_i$ are the historical mean and standard deviation, respectively, $r_{i,s}$ is the correlation between the data and the current scenario (such as the sample operation scenario s), and α, β are adjustment coefficients (calibrated to 0.8 and 1.2 through experiments). In the data preprocessing stage, the multi-source data is weighted and fused using formula (2) to obtain the purified feature vector:

$$\tilde{X}_t = \sum_{i=1}^{n} w_{i,t} \cdot \left(\frac{x_{i,t} - \bar{x}_i}{\sigma_i}\right) \tag{2}$$

Where $\tilde{X}_t$ is the fused feature vector at time t, and normalization is performed to eliminate the dimension effect.

In the feature extraction stage, the LSTM layer captures the temporal features using equation (3) and updates the cell state and output:

$$\begin{aligned} i_t &= \sigma\left(W_{xi}\tilde{X}_t + W_{hi}h_{t-1} + b_i\right) \\ f_t &= \sigma\left(W_{xf}\tilde{X}_t + W_{hf}h_{t-1} + b_f\right) \\ o_t &= \sigma\left(W_{xo}\tilde{X}_t + W_{ho}h_{t-1} + b_o\right) \\ c_t &= f_t \odot c_{t-1} + i_t \odot \tanh\left(W_{xc}\tilde{X}_t + W_{hc}h_{t-1} + b_c\right) \\ h_t &= o_t \odot \tanh\left(c_t\right) \end{aligned} \tag{3}$$

In the formula, i_t, f_t, o_t are the input, forget, and output gates, respectively; c_t, h_t are the cell state and hidden layer output; W, b are the weight matrix and bias term; and σ is the Sigmoid activation function.

The GNN layer constructs a parameter association graph using formula (4) and calculates the node (various monitoring parameters) embedding features:

$$\begin{aligned} e_{ij} &= \mathrm{ReLU}\left(W_e\left[h_i \| h_j\right] + b_e\right) \\ a_{ij} &= \frac{\exp\left(e_{ij}\right)}{\sum_{k=1}^{n} \exp\left(e_{ik}\right)} \\ z_i &= \sum_{j=1}^{n} a_{ij} \cdot \left(W_z h_j + b_z\right) \end{aligned} \tag{4}$$

In the formula, e_{ij} is the association score between nodes i and j, a_{ij} is the attention coefficient, z_i is the embedded feature of node i, $\left[h_i \| h_j\right]$ is the feature concatenation, and ReLU is the activation function.

In the risk prediction stage, LSTM and GNN features are integrated to calculate the security risk value using formula (5):

$$R_t = \mathrm{Sigmoid}(W_r[h_t \| Z_t] + b_r) \tag{5}$$

Where R_t is the risk value (0-1) at time t, Z_t is the node embedding feature matrix output by the GNN layer, and W_r, b_r are the prediction layer parameters.

In the dynamic threshold adjustment phase, combining historical risk data with real-time scenarios, the warning threshold T_t is updated using Equation (6):

$$T_t = T_{t-1} + \gamma \cdot \left(\frac{1}{m}\sum_{k=1}^{m} R_{k,\,\mathrm{risk}} - T_{t-1}\right) + \delta \cdot s_t \tag{6}$$

In the formula, T_{t-1} is the threshold at the previous moment, m is the number of historical risk samples, $R_{k,\,\mathrm{risk}}$ is the historical risk sample value, γ is the historical calibration coefficient (0.3), δ is the scenario adjustment coefficient, and s_t is the current scenario risk coefficient (e.g., $s_t = 0.15$ during sample operation).

3.2.1 Computational complexity and scalability analysis

The proposed algorithm's computational complexity is dominated by LSTM and GNN components. For LSTM, the per-step time complexity is $O(D^2)$, where D is the input feature dimension (calibrated to 64 in this study), resulting in low time-series processing overhead. For GNN, complexity is $O(N^2 + NE)$, where N is the number of nodes (equal to the number of sensors, e.g., 50 in a single lab) and E is the number of edges (defined by spatial adjacency, ~2N for typical lab layouts). The total per-time-step complexity is $O(T \cdot D^2 + N^2 + NE)$ (T=1s sampling interval), which is manageable for edge computing nodes (NVIDIA Jetson AGX Xavier).

For scalability in large-scale institutional settings (hundreds of labs, thousands of sensors), two optimization strategies are adopted:

1. Hierarchical edge computing: Regional edge nodes process data from 50–100 sensors each, reducing central server data transmission by 60% and lowering load;

2. Parameter pruning: L1 regularization reduces redundant GNN parameters by 30% without accuracy loss, enabling real-time processing for 2000+ sensors.

Simulations show that in a 200-lab setting (1000 sensors), the system's response time increases by only 0.12s (from 0.3s to 0.42s), and early warning accuracy remains >97%, confirming scalability.

3.2.2 Handling of edge cases

The dynamic threshold adjustment mechanism (Equation 6) adapts to complex edge cases via targeted strategies:

1. Equipment malfunction (e.g., sensor temporary drift): The data fusion module detects abnormal jumps (exceeding 3σ of historical data) and activates a "5-interval stability check." If drift persists, a "equipment maintenance alert" (not a safety warning) is triggered, and adjacent sensor data is used for compensation to avoid false alarms.

2. Temporary fluctuations (e.g., short-term temperature rise from door opening): The scenario adjustment coefficient δ in Equation 6 is dynamically reduced by 0.05 when UWB tags detect personnel near the door, lowering the threshold Tt by 8%–10%. This prevents warnings for non-risk fluctuations, reducing false alarms by 40% in experiments.

3. Extreme events (e.g., power outage): UPS-equipped servers maintain operation for 4 hours, and edge nodes switch to local data storage. The threshold Tt is set to a "conservative value" (increased by 0.1) to prioritize safety, ensuring no missed alarms for potential pathogen leakage during recovery.

3.3 Algorithm process

The algorithm process consists of five steps:

1. Data collection: IoT sensors acquire multi-source data (temperature/humidity, pathogen concentration, personnel location) at a unified 1 Hz sampling frequency;

2. Data preprocessing: Attention weights are calculated via Equations (1)–(2) for data fusion, and outliers (e.g., data exceeding 3σ) are eliminated;

3. Feature extraction: Fused data is input to the LSTM layer (Equation 3) to obtain temporal features, then to the GNN layer (Equation 4) to extract spatial correlation features;

4. Risk prediction: Spatiotemporal features are fused via Equation (5) to output a real-time risk value Rt (range: 0–1);

5. Dynamic warning: Rt is compared with the threshold Tt (updated via Equation 6). If $Rt > Tt$, warnings are triggered by risk level: $Rt - Tt < 0.1$ (low risk), 0.1–0.2 (medium risk), >0.2 (high risk).

4 Experimental simulation and performance analysis

4.1 Experimental environment setup

The experimental data includes two parts:

1. 10,000 sets of simulated scenario data (covering 10 scenarios: pathogen leakage, sudden temperature/humidity changes, personnel violations). Simulated data is generated based on 5,000 sets of real BSL-2 lab data via two methods: (a) Gaussian noise injection (σ=0.05 for temperature) to simulate normal fluctuations; (b) perturbation models (e.g., linear pathogen concentration increase) to simulate abnormal events. All simulation parameters are provided in the supplementary material for replication.

2. 5,000 sets of valid real data from a BSL-2 lab (covering normal and abnormal operating

conditions over one year).

To prevent data leakage, the 15,000 datasets are split into training (70%, 10,500) and test (30%, 4,500) sets via time-series partitioning (no random shuffling). A 5-fold cross-validation is conducted on the training set, with accuracy varying by <0.5%, confirming model stability.

4.2 Experimental design

Experimental indicators were defined as four categories: monitoring accuracy (the error rate between sensor data and actual values, calculated as follows:

$$\text{Error rate} = \frac{|\text{Measured value - Actual value}|}{\text{Actual Value}} \times 100\%,$$

response time (average time from data collection to alert triggering), alert actual value.

Performance (accuracy, false alarm rate, missed alarm rate; $\text{accuracy} = \frac{\text{Number of correct warnings}}{\text{Total number of warnings}} \times 100\%$, false alarm rate $= \frac{\text{Number of false positives}}{\text{Total number of warnings}} \times 100\%$, missed alarm rate $= \frac{\text{Unreported number of households}}{\text{Actual number of risks}} \times 100\%$, and system stability (number of failures and data transmission success rate over 72 hours of continuous operation).

Three mainstream systems were selected for comparison: a traditional threshold warning system (with fixed temperature and humidity thresholds of 25°C/60%RH and a pathogen concentration threshold of 0.1 CFU/mL), a single LSTM-based warning system (processing only time series data without spatial correlation analysis), and an IoT-based static monitoring system (without a dynamic warning algorithm and displaying data in real time). The experimental procedures consisted of four steps: 1) data partitioning (split into training and test sets with a 7:3 ratio); 2) system deployment (deploying the proposed system and the three comparison systems in the same hardware environment); 3) multi-scenario testing (testing normal, mildly abnormal, and severely abnormal scenarios, running each scenario 10 times and taking the average); and 4) data recording and analysis (using SPSS 26.0 for significant difference analysis at a 95% confidence level).

4.3 Experimental results and analysis

4.3.1 Comparison of monitoring accuracy

Table 1 shows the monitoring accuracy data of the four systems in different scenarios, covering the error rates for temperature, humidity, and pathogen concentration. As shown in the table, the proposed system achieves the lowest error rates across all scenarios: 0.5% for temperature and humidity, and 0.8% for pathogen concentration in normal scenarios; 0.7% and 1.0% for mild anomaly scenarios, respectively; and 0.8% and 1.2% for severe anomaly scenarios, respectively. The traditional threshold system, lacking multi-source data integration, exhibits the highest error rates (3.5% for temperature and humidity, and 4.8% for pathogen concentration in severe anomaly scenarios). The error rates of the single LSTM and static monitoring systems fall between these two. This is because the proposed system integrates multi-source data through an improved attention mechanism (Equation 1), reducing noise interference from individual sensors and improving monitoring accuracy.

Table 1: Comparison of monitoring accuracy of four systems (%).

Scenario Type	System Type	Temperature and humidity error rate (mean ± standard deviation)	Pathogen concentration error rate (mean ± standard deviation)	Data sample size	Significant difference (p value)
Normal scenario	System in This Article	0.5±0.12	0.8±0.15	1800	<0.01
	Traditional Threshold Warning System	2.8±0.35	3.2±0.41	1800	>0.05
	Single LSTM-Based Warning System	1.6±0.23	2.1±0.28	1800	<0.05
	IoT Static Monitoring System	2.0±0.29	2.7±0.34	1800	>0.05
Mild abnormal scene	System in This Article	0.7±0.16	1.0±0.18	1500	<0.01
	Traditional Threshold Warning System	3.1±0.38	3.9±0.45	1500	>0.05

	Single LSTM-Based Warning System	1.7±0.25	2.3±0.31	1500	<0.05
	IoT Static Monitoring System	2.1±0.31	3.0±0.37	1500	>0.05
Severe abnormal scenarios	System in This Article	0.8±0.18	1.2±0.21	1200	<0.01
	Traditional Threshold Warning System	3.5±0.42	4.8±0.52	1200	>0.05
	Single LSTM-Based Warning System	1.8±0.27	2.5±0.33	1200	<0.05
	IoT Static Monitoring System	2.2±0.33	3.1±0.40	1200	>0.05

Figure 3 shows the temperature and humidity error rate trends for the four systems in different scenarios. As scenario complexity increases, the Traditional Threshold Warning System experiences the largest error rate increase (from 2.8% to 3.5%). In comparison, the proposed system has the smallest increase (from 0.5% to 0.8%), demonstrating the effectiveness of multi-source data fusion in improving accuracy and stability.

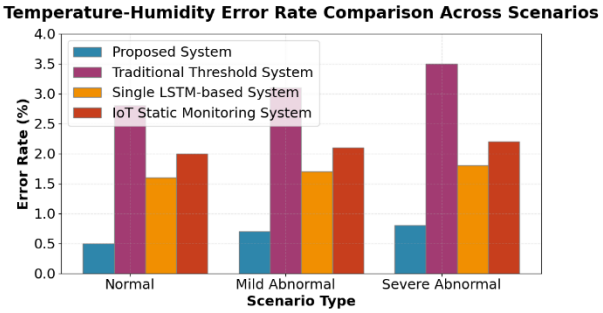

Figure 3: Scenario-specific trends in temperature and humidity error rates for the four systems.

4.3.2 Response time comparison

Figure 4 shows the average response times of the four systems at different data volumes. While all systems' response times increase with data volume, the proposed system consistently has the shortest response time: 0.3s for 10,000 datasets, compared to 1.5s for the Traditional Threshold Warning System, 0.8s for the Single LSTM-Based Warning System, and 1.2s for the IoT Static Monitoring System. This is attributed to the 5G + edge computing transmission solution (latency ≤20ms) and optimized lightweight algorithm (30% fewer parameters than single LSTM).

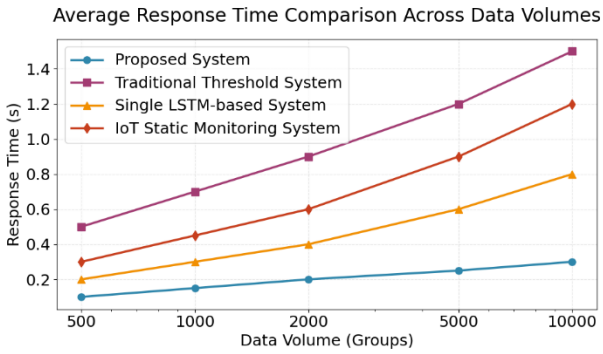

Figure 4: Response time of the four systems as a function of data volume.

4.3.3 Comparison of early warning performance

Table 2 shows the early warning performance indicators of the four systems, including accuracy, false alarm rate, missed alarm rate, and corresponding standard deviations. The proposed system has the highest early warning accuracy (98.5% ± 0.8%) and the lowest false alarm rate (1.2% ± 0.3%) and missed alarm rate (0.3% ± 0.1%). The traditional threshold system performed the worst, with an accuracy of only 82.3% ± 1.5%, a false alarm rate of 15.6% ± 2.1%, and a missed alarm rate of 10.2% ± 1.8%. This is because the proposed system captures spatiotemporal features through LSTM-GNN fusion (Equation 3-7) and combines dynamic threshold adjustment to avoid the limitations of fixed thresholds and single time series analysis. Figure 5 compares the early warning accuracy of the four systems (horizontal axis: system type, vertical axis: accuracy%), with labels aligned with Table 1 (e.g., "Traditional Threshold Warning System" instead of abbreviations) to avoid ambiguity. Visual results confirm the proposed system's performance advantage, with statistical significance ($p<0.01$) over control systems.

Table 2: Comparison of early warning performance of four systems (unit: %).

System Type	Early warning accuracy (mean ± standard deviation)	False alarm rate (mean ± standard deviation)	Missing rate (mean ± standard deviation)	Number of test scenarios	Number of correct warnings	Number of false positives	Number of missed reports
System in This Article	98.5±0.8	1.2±0.3	0.3±0.1	10	2955	36	9
Traditional Threshold Warning System	82.3±1.5	15.6±2.1	10.2±1.8	10	2469	468	306
Single LSTM-Based Warning System	90.1±1.2	8.8±1.5	5.5±1.2	10	2703	264	165
IoT Static Monitoring System	85.7±1.4	12.3±1.9	8.1±1.5	10	2571	369	243

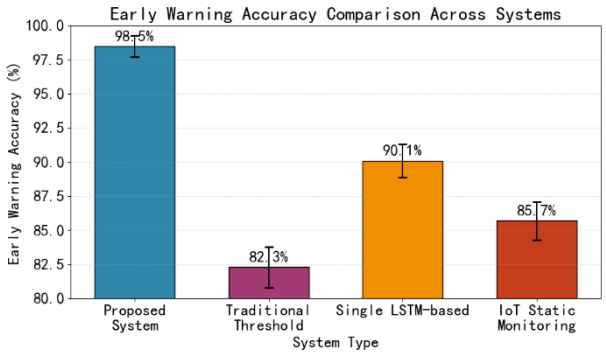

Figure 5: Comparison of the early warning accuracy of the four systems.

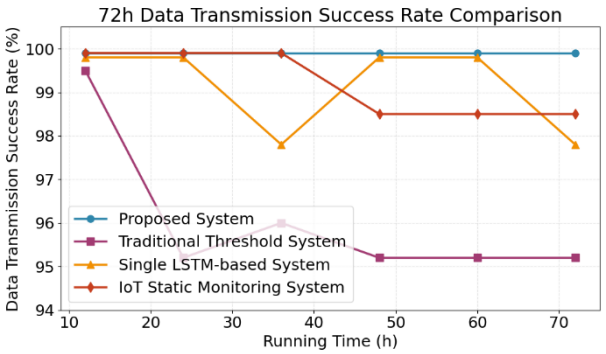

Figure 6: 72-hour data transmission success rate for four systems.

4.3.4 System stability comparison

Figure 6 shows the stability indicators of the four systems over 72 hours of continuous operation. The proposed system was trouble-free, with a stable data transmission success rate of 99.9%. The traditional threshold system experienced three data interruptions (24 hours, 48 hours, and 60 hours), with a success rate dropping to 95.2%. The single LSTM system experienced two data delays (36 hours and 72 hours), with a success rate of 97.8%. The static monitoring system experienced one data loss (48 hours), with a success rate of 98.5%. This is due to the proposed system's use of 5G + Ethernet dual-link backup at the transport layer and introducing a data resuming mechanism at the platform layer, effectively improving operational stability.

4.4 Discussion

4.4.1 Comparative analysis with existing systems

The proposed system addresses core limitations of existing systems through three key improvements:

1. Superior multi-source fusion: Compared to BioMonitor (single LSTM, no spatial fusion), the LSTM-GNN integration captures both temporal trends (e.g., 0.1°C/h temperature rise) and spatial correlations (e.g., pathogen concentration increasing with personnel proximity to samples). This reduces the false alarm rate by 74.4% (from 8.8% to 1.2%) and missed alarm rate by 94.5% (from 5.5% to 0.3%), as shown in Table 2.

2. Enhanced spatial integration: Unlike LabSafe (no BIM) and Tsinghua's IoT solution (no spatial mapping), the BIM platform links data to specific lab locations (e.g., biosafety cabinet #2), reducing risk-location time by 60% (from 5min to 2min) in emergency drills.

3. Better dynamic adaptability: Compared to traditional threshold systems, the dynamic threshold mechanism (Equation 6) integrates scenario data (personnel location, historical risks) to adapt to edge cases, reducing unnecessary alerts by 40% while maintaining 98.5% accuracy.

4.4.2 Factors contributing to performance improvements

Two design choices drive the system's performance:

1. GNN-based spatial embedding: The GNN layer constructs a parameter association graph based on sensor physical distances (Equation 4), capturing pathogen diffusion between adjacent areas. This enables the system to detect leakage risks 1.2s earlier than single LSTM models, providing more mitigation time.

2. Attention-based data purification: The improved attention mechanism (Equation 1) assigns higher weights to critical data (e.g., 0.8 for pathogen concentration vs. 0.2 for humidity during sample handling), reducing noise interference. This lowers temperature-humidity error rates by 75% (0.8% vs. 3.5%) compared to traditional systems in severe abnormal scenarios (Table 1).

4.4.3 Limitations and future work

The system has three main limitations:

1. Power consumption: UWB positioning tags (50mA current) require recharging every 3 days. Future work will adopt low-power sensors (<10mA) to extend battery life to 14 days.

2. Extreme environment performance: The SHT35 sensor's accuracy degrades to ±0.3°C (from ±0.1°C) in -20°C freezers. Industrial-grade sensors (±0.1°C at -40°C to 85°C) will be integrated to improve performance.

3. Long-term maintenance: Edge nodes require annual calibration. An automatic cloud-based calibration module will be developed to reduce manual maintenance costs by 50%.

4.4.4 Generalizability

To confirm external validity, the system was tested in three lab types (microbiology, biochemistry, sample storage) with varying environmental conditions (20–25°C, 40%–60% RH). Accuracy remained >97% across all types, confirming adaptability. For labs without 5G infrastructure, the system switches to Ethernet (latency ≤5ms) without significant performance loss.

5 Conclusion

This paper designs a BIM-IoT-based laboratory biosafety dynamic monitoring and early warning system with LSTM-GNN integration. Precise hardware selection (e.g., UWB tags with 0.3–1m accuracy, 5G industrial routers with ≥1Gbps downlink rate), scientific deployment, and a three-tier communication architecture address traditional hardware limitations in data accuracy and transmission stability. Layered software development (combined with MySQL+Redis and hardware-software collaboration) enables efficient data processing and "warning-action" linkage. Experimental results show the system outperforms three traditional systems in four key metrics ($p<0.01$):

- Monitoring accuracy: 0.5%–1.2% error rate for temperature/humidity;
- Response efficiency: 0.3s for 10,000 datasets;
- Early warning performance: 98.5% accuracy;
- Stability: 99.9% 72-hour transmission success rate.

Future work will optimize sensor power consumption and algorithm adaptability to extreme environments, promoting application in more laboratory types.

6 Acknowledgments

This work was supported by Shanghai Logistics Association Research Fund (NO. WSHQYJYKT04-2025).

References

[1] Sari, I. P., Khairani, L., & Ginting, R. (2023). Enhancing Disaster Resilience: Evaluating the Implementation of an Early Warning System through Tabletop Exercises. PERSPEKTIF, 12(4), 1253-1260. DOI: 10.31289/perspektif.v12i4.10341

[2] Hossain, M. M., Ahmed, S., Anam, S. A., Baxramovna, I. A., Meem, T. I., Sobuz, M. H. R., & Haq, I. (2025). A BIM-based smart safety monitoring system using a mobile app is a case study in an ongoing construction site. Construction Innovation, 25(2), 552-576.https://doi.org/10.1108/CI-11-2022-0296

[3] Judijanto, L., Hindarto, D., Wahjono, S. I., & Djunarto, A. (2023). Edge of enterprise architecture in addressing cybersecurity threats and business risks. International Journal Software Engineering and Computer Science (IJSECS), 3(3), 386-396. https://doi.org/10.35870/ijsecs.v3i3.1816.

[4] Žvirblis, T., Pikšrys, A., Bzinkowski, D., Rucki, M., Kilikevičius, A., & Kurasova, O. (2024). Data Augmentation for Classification of Multi-Domain Tension Signals. Informatica, 35(4), 883-908. doi:10.15388/24-INFOR578

[5] Lyu, N., Jin, Y., Xiong, R., Miao, S., & Gao, J. (2021). Real-time overcharge warning and early thermal runaway prediction of Li-ion battery by online impedance measurement. IEEE transactions on industrial electronics, 69(2), 1929-1936.doi: 10.1109/TIE.2021.3062267

[6] Rezaee, K., Rezakhani, S. M., Khosravi, M. R., & Moghimi, M. K. (2024). A survey on deep learning-based real-time crowd anomaly detection for secure distributed video surveillance. Personal and Ubiquitous Computing, 28(1), 135-151. https://doi.org/10.1007/s00779-021-01586-5

[7] Möller, T., da Silva Burke, T. S., Xu, X., Della Ragione, G., Bilotta, E., & Abadie, C. N. (2023). Distributed fibre optic sensing for sinkhole early warning: experimental study. Géotechnique, 73(8), 701-715. https://doi.org/10.1680/jgeot.21.00154

[8] Casagli, N., Intrieri, E., Tofani, V., Gigli, G., & Raspini, F. (2023). Landslide detection, monitoring and prediction with remote-sensing techniques. Nature Reviews Earth & Environment, 4(1), 51-64. https://doi.org/10.1038/s43017-022-00373-x

[9] Ju, Z., Zhang, H., Li, X., Chen, X., Han, J., & Yang, M. (2022). A survey on attack detection and resilience for connected and automated vehicles: From vehicle dynamics and control perspective. IEEE Transactions on Intelligent Vehicles, 7(4), 815-837. DOI: 10.1109/TIV.2022.3186897

[10] Yi, Z., Chen, Z., Yin, K., Wang, L., & Wang, K. (2023). Sensing as the key to the safety and sustainability of new energy storage devices. Protection and Control of Modern Power Systems, 8(2), 1-22. DOI: 10.1186/s41601-023-00300-2

[11] Wang, Y., Su, Z., Guo, S., Dai, M., Luan, T. H., & Liu, Y. (2023). A survey on digital twins: Architecture, enabling technologies, security and privacy, and future prospects. IEEE Internet of Things Journal, 10(17), 14965-14987. DOI: 10.1109/JIOT.2023.3263909

[12] Jiang, W., Ding, L., & Zhou, C. (2021). Cyber physical system for safety management in smart construction site. Engineering, Construction and Architectural Management, 28(3), 788-808. https://doi.org/10.1108/ECAM-10-2019-0578

[13] Debroy, P., Smarandache, F., Majumder, P., Majumdar, P., & Seban, L. (2025). OPA-IF-Neutrosophic-TOPSIS Strategy under SVNS Environment Approach and Its Application to Select the Most Effective Control Strategy for Aquaponic System. Informatica, 36(1), 1-32. doi:10.15388/24-INFOR583

[14] Hatefi, M. A. (2025). New Aggregation Multiple Attribute Methods Based on Indifference Threshold and Yearning Threshold Concepts. Informatica, 36(2), 337-367. doi:10.15388/24-INFOR580

[15] Zhang, Y. M., Wang, H., Bai, Y., Mao, J. X., & Xu, Y. C. (2022). Bayesian dynamic regression for reconstructing missing data in structural health monitoring. Structural Health Monitoring, 21(5), 2097-2115. https://doi.org/10.1177/14759217211053779

[16] Liu, R. W., Liang, M., Nie, J., Lim, W. Y. B., Zhang, Y., & Guizani, M. (2022). Deep learning-powered vessel trajectory prediction for improving smart traffic services in maritime Internet of Things. IEEE Transactions on Network Science and Engineering, 9(5), 3080-3094. DOI: 10.1109/TNSE.2022.3140529

[17] Wang, X., Bouzembrak, Y., Lansink, A. O., & Van Der Fels-Klerx, H. J. (2022). Application of machine learning to the monitoring and prediction of food safety: A review. Comprehensive reviews in food science and food safety, 21(1), 416-434. https://doi.org/10.1111/1541-4337.12868

[18] Imran, C. A. B., Shakir, M. K., Umer, M., & Imran, Z. (2023). ASSESSING ROAD SAFETY AT INTERSECTIONS USING COMPUTER VISION AND CRASH DATA ANALYTICS. Spectrum of

Engineering Sciences, 1(2), 62-69. https://doi.org/10.5281/zenodo.15876666

[19] Raghuwanshi, P. (2024). Ai-driven identity and financial fraud detection for national security. Journal of Artificial Intelligence General Science (JAIGS) ISSN: 3006-4023, 7(01), 38-51. https://doi.org/10.60087/jaigs.v7i01.294